5.1) Introduction

Couplers are the most fundamental building blocks in guided-wave optics. They are devices that can split optical power in required ratios between multiple waveguides. Three coupler configurations can be identified, namely the bi-directional coupler, the multi-mode interference coupler (MMI coupler) and the star coupler. Whereas the bi-directional coupler can only split optical power between two waveguides, the MMI- and star couplers can split the power between more than two waveguides.

5.2) The bi-directional coupler

Bi-directional couplers can split optical power between two waveguides in any ratio required. Although the number of outputs might be restrictive, this coupler is the only one (in its basic form) that can split the power in a ratio other than P/N, where P is the input power and N is the number of output channels.

Bi-directional couplers are formed by placing two waveguides in close proximity to one another. The coupling occurs as a result of the overlap between the evanescent field of the one waveguide and the core of the other waveguide, as indicated in figure 5.1, where the green lines represent the electromagnetic fields. Several theoretical analyses of directional couplers have been reported [1,2]. However, it is difficult to achieve a device without experimental results [3], because of its sensitivity to manufacturing variations. Simulations utilizing BPM can help bridge the gap between theory and practice, and supply a very good first-order approximation of how the planar circuit will behave, as well as aid in the optimisation of the circuit.

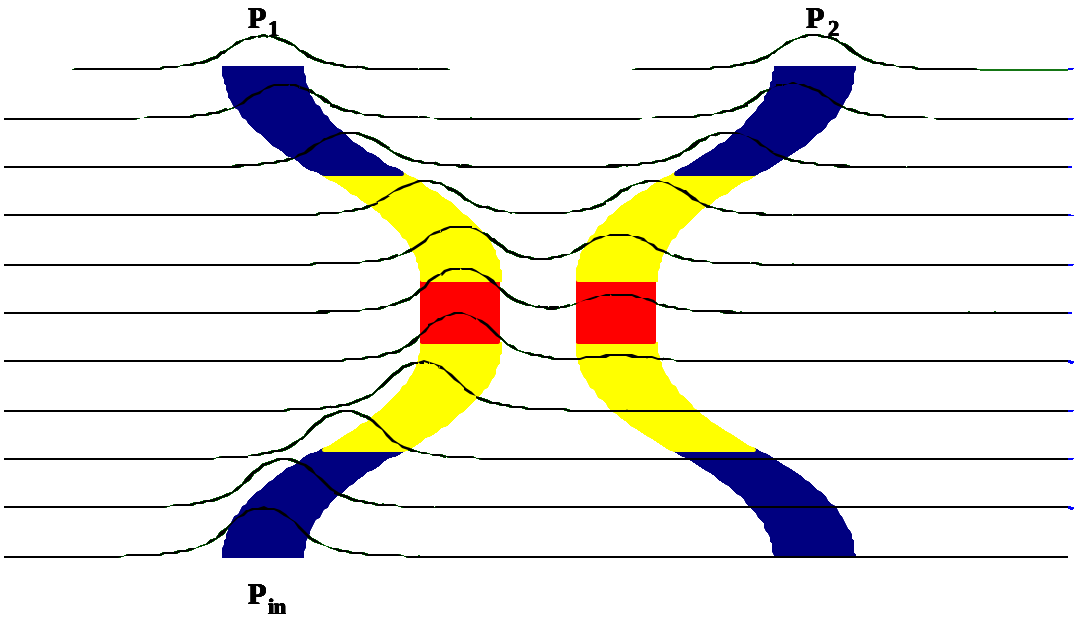

Figure 5.1: Geometrical layout of a bi-directional coupler, where $P_{in} = P_1 + P_2$

5.2.1) Theoretical aspects

As was stated, an overlap of evanescent fields with the waveguides is required in order to obtain coupling. For the coupling coefficient to be sufficiently large, the tail of the evanescent field has to reach a significant region of the waveguide. It is thus clear that the spacing between the waveguides has the largest effect on the coupling coefficient [4]. It is also important to note that the coupling coefficient depends exponentially on this spacing because of the exponential decay of the evanescent fields [4]. A general rule of thumb is to set the spacing of the main coupling regions in the order of a waveguide width.

The power coupling ratio can be described by [3,4,5] as

$$h = \sin^2\left[\frac{p}{2}\frac{L + L_{end}}{L_c}\right] \tag{5.1}$$

where L is the length of the straight coupling section, L_{end} is the increase in coupling length in the transition area, and L_c is the total coupling length needed to completely couple light from one waveguide to the other, given by

$$L_c = \frac{2p}{coupling\_coefficient} \tag{5.2}$$

The coupling coefficient as stated above can be solved by using the coupled mode equations. Furthermore, it can be shown that [5]

$$L_{end} = \sqrt{pRd_0} \tag{5.3}$$

where R is the radius of curvature in the s-bend region, and d_0 and L_0 are phenomenological variables obtained from [5]

$$L_c \approx L_0 e^{d/d_0} \tag{5.4}$$

where d is the separation of the waveguides in the straight coupling section.

It is possible to obtain the values of L_c and L_{end} by simulation. This is done by comparing the fraction of crossed power of two couplers with different L but at the same wavelength [5]. From here, d_0 can be obtained. This procedure can be repeated for various wavelengths in order to obtain a set of L_c '*s* and L_{end} '*s* for prediction purposes. This methodology is described in section 5.2.3.

5.2.2) Coupler design

Two couplers were designed in the BeamPROP environment utilising the waveguide parameters as set out in section 4.2. The physical dimensions of the couplers are summed up in figure 5.2. It should be noted that the bending radius is well within the bounds set in section 4.3 for the minimum-bending radius.

In figures 5.3 and 5.4, the couplers' simulated responses to changes in the straight coupling length (L) are presented. The losses for these devices are negligible, as can be seen from the graphs. It can be seen, for example, that for a coupling ratio of 50%, a length of $\pm 244.5\mu m$ for Coupler 1 and $\pm 256.2\mu m$ for Coupler 2 is required at a wavelength of 1550nm. The final dimensions for a 3dB coupler as designed in the BeamPROP CAD environment are then $1120\mu m \times 12.8\mu m$ for Coupler 1 and $2000\mu m \times 24.3\mu m$ for Coupler 2.

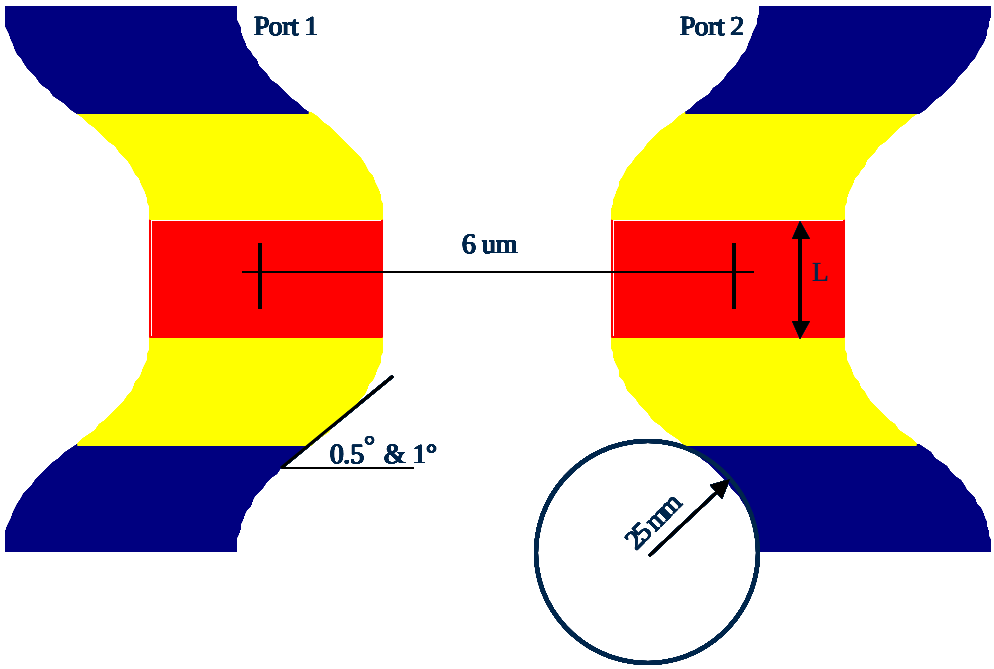

Figure 5.2: Physical layout of designed couplers

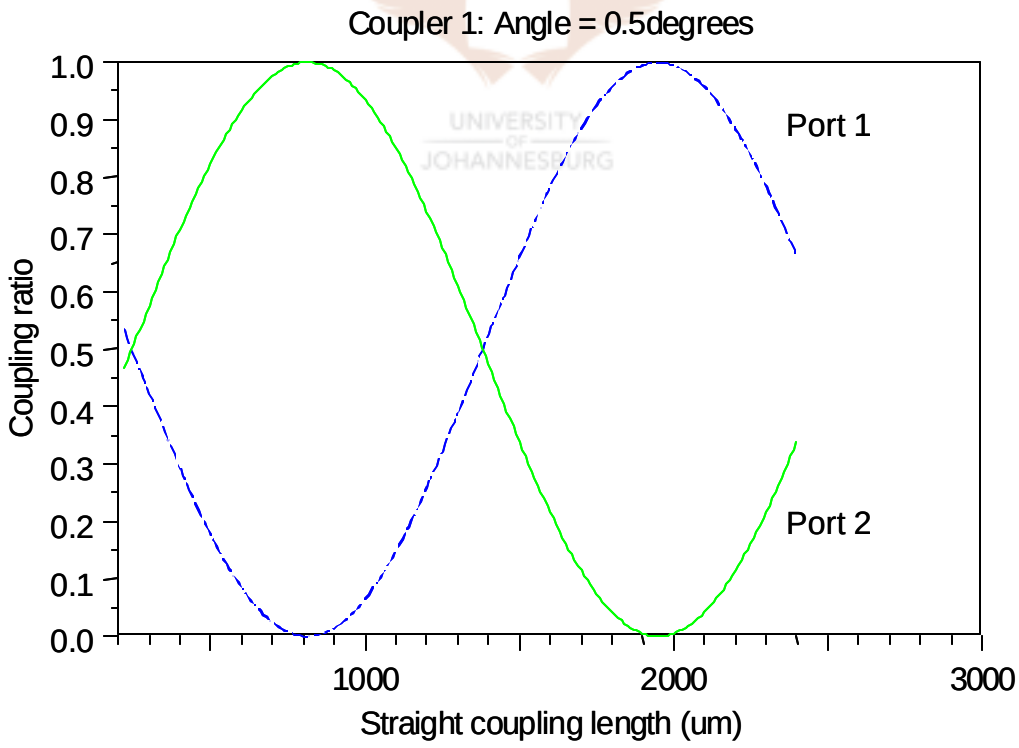

Figure 5.3: Simulation results for Coupler 1

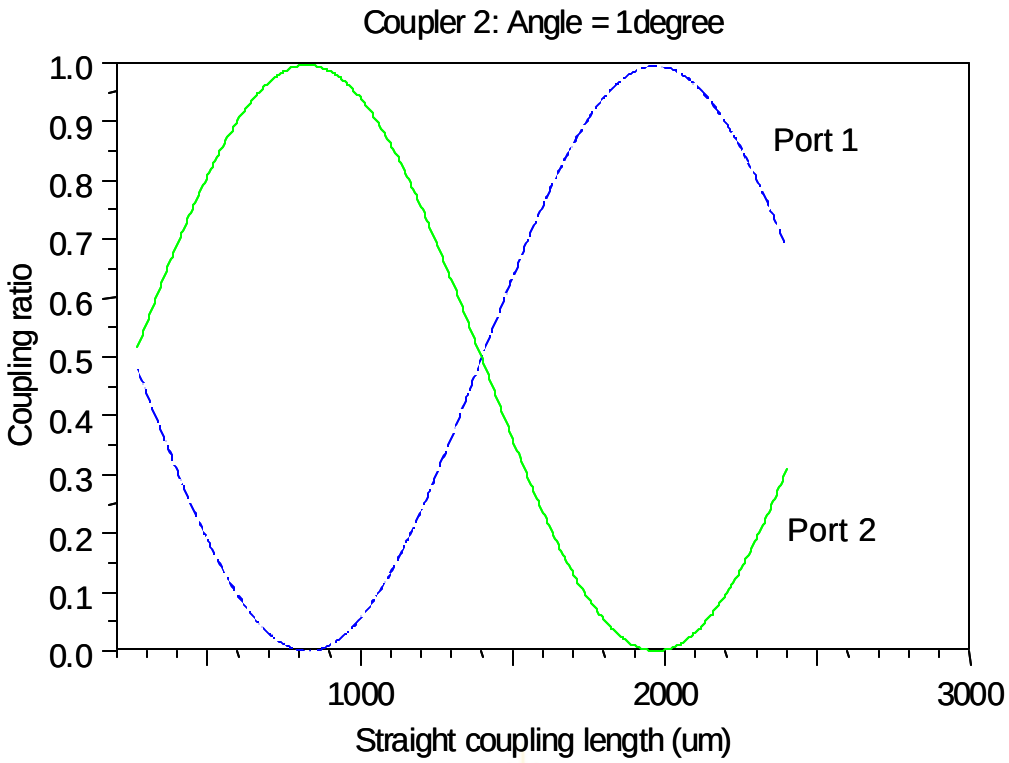

Figure 5.4: Simulation results for Coupler 2

5.2.3) Restrictions of the BPM simulations

As was stated in section 4.3, the simulated bend method allows for the simulation of large bending angles in the BeamPROP environment. In the case of the directional coupler, however, this method cannot be employed due because the separation effects are not incorporated in the simulated bend technique. In other words, after transformation, the coupling occurs as it would in the straight coupling length area, which will result in an erroneous simulation output.

If a bending radius of 1.5mm were to be used in conjunction with an arc angle of 3°, a coupler measuring 560µm × 17.3µm would be obtained, which is about half the length of the dimensions stated above. For the purposes of this thesis, where the couplers will be used in filter configurations, the coupler with the larger bending radius is used to allow for direct simulation.

If the smallest possible size is, however, a pre-defined criterion, the dependence of L_c and L_{end} on the angle and bending radius can be predicted by using the theory defined

in section 5.2.1. As was stated, a value for L_c can be obtained by varying the parallel length L and recording the output ratio. From standard algebra, the following formulae have been derived:

$$L_c = \frac{p\left(L_1 - L_2\right)}{2\left(\arcsin\sqrt{h_1} - a\sin\sqrt{h_2}\right)} \tag{5.5}$$

$$L_{end} = \frac{2\arcsin\sqrt{h_1}}{p} L_c - L_1 \tag{5.6}$$

It is important to note that equations 5.5 and 5.6 can only be used for one wavelength at a time. Bearing this in mind, simulations were performed in BeamPROP for Coupler 1. The length L was varied at L_1 = 250µm and L_2 = 300µm for wavelengths between 1.5µm and 1.604µm. In figures 5.5 and 5.6, the simulation results for the above procedure are presented.

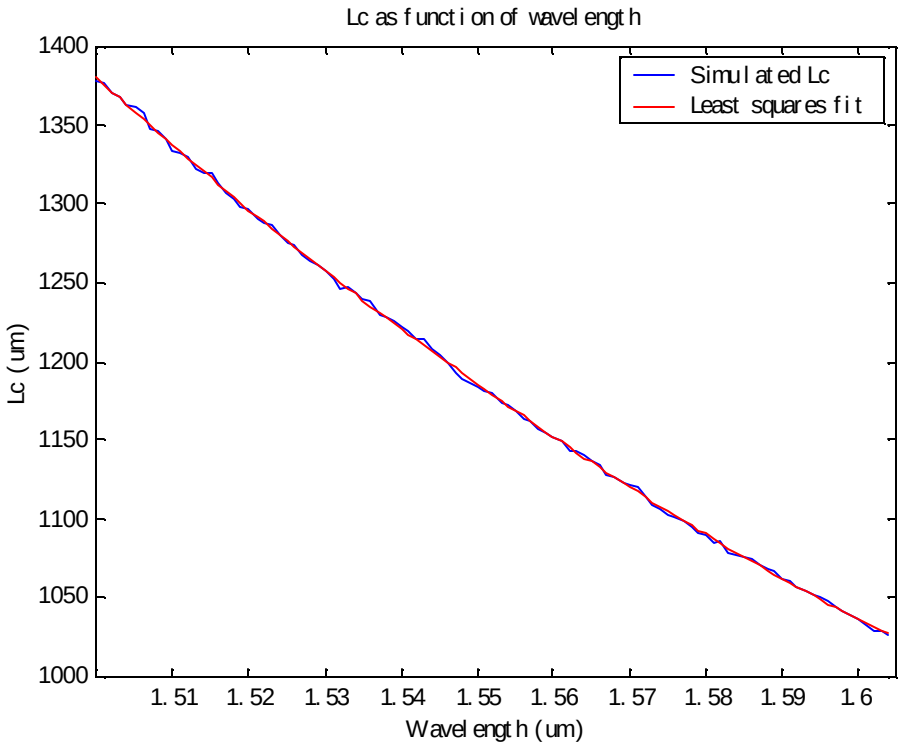

Figure 5.5: Simulated L_c as a function of wavelength

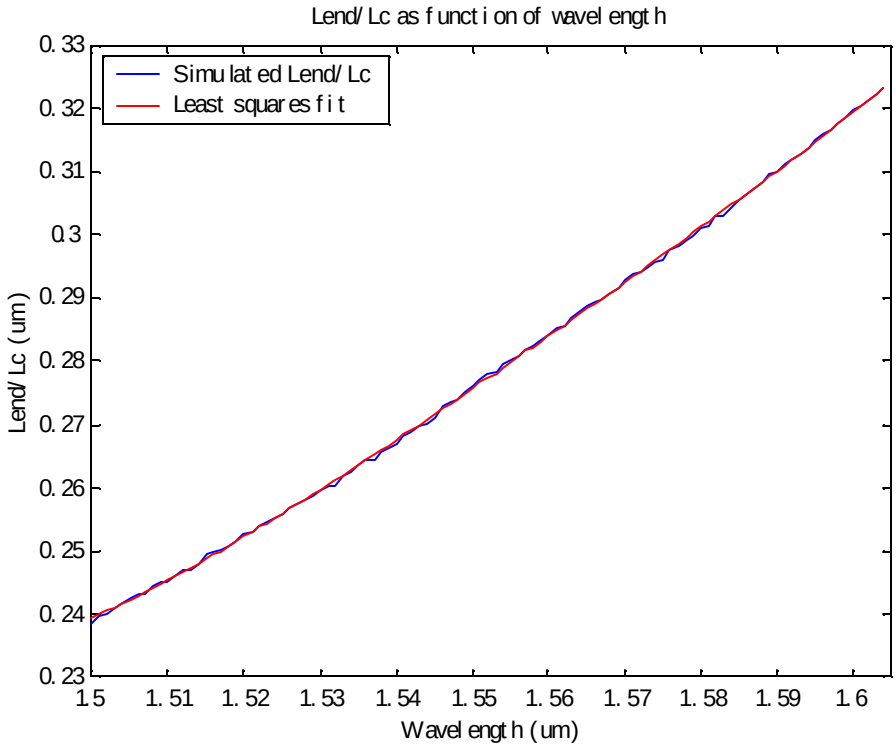

Figure 5.6: Simulated L_{end}/L_c as a function of wavelength

To obtain a downscaling prediction, the waveguide separation in the transition areas defined by L_{end} is investigated. In figure 5.7, the geometrical layout of a curved waveguide used in the coupler is shown. By substituting the design parameters of Coupler 1 into the equations given in figure 5.7, the value of b is found to be 0.95µm. So, in order to use the results of figures 5.5 and 5.6, the angle corresponding to values of radius R is given by:

$$q = \arccos\left(\frac{0.95 - R}{R}\right) \tag{5.7}$$

As an example, if R = 20000µm, an angle of q = 0.56° is obtained. A simulation was run in which the validity of these results was verified successfully. In conclusion, then, if the minimum bending radius of 1500µm is to be used, the corresponding angle will be 2.04°. A coupler with these dimensions will have the same simulation results as Coupler 1.

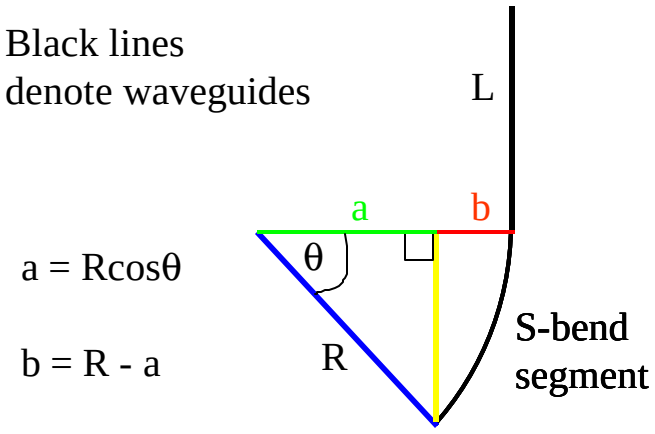

Figure 5.7: Dependence of curved waveguides on R and q

5.3) Multi-mode interference couplers

Multi-mode interference (MMI) couplers are based on the self-imaging property of multi-mode propagation in a slab. Self-imaging, also known as the Talbot effect, requires that the medium of propagation have an associated periodicity [4]. In multimode waveguides, the input field excites a number of modes. If the propagation constants of the modes are integer multiples of a constant $2p/L_0$, the self-imaging occurs at distances that are integer multiples of L_0.

Figure 5.8 depicts the physical layout of an MMI coupler. These couplers can be used to split light into more than two paths, and can also split the light in arbitrary ratios, as shown by Besse et al [4]. MMI couplers can be used in tuneable Mach-Zehnder couplers (discussed in section 6.6), and have also been demonstrated as building blocks in arrayed waveguide gratings (AWGs) [6, 7], albeit in smaller systems because the number of output waveguides is limited by geometrical constraints. In general they are more robust than bi-directional couplers from a manufacturing viewpoint (due to the absence of bending elements), but exhibit higher losses.

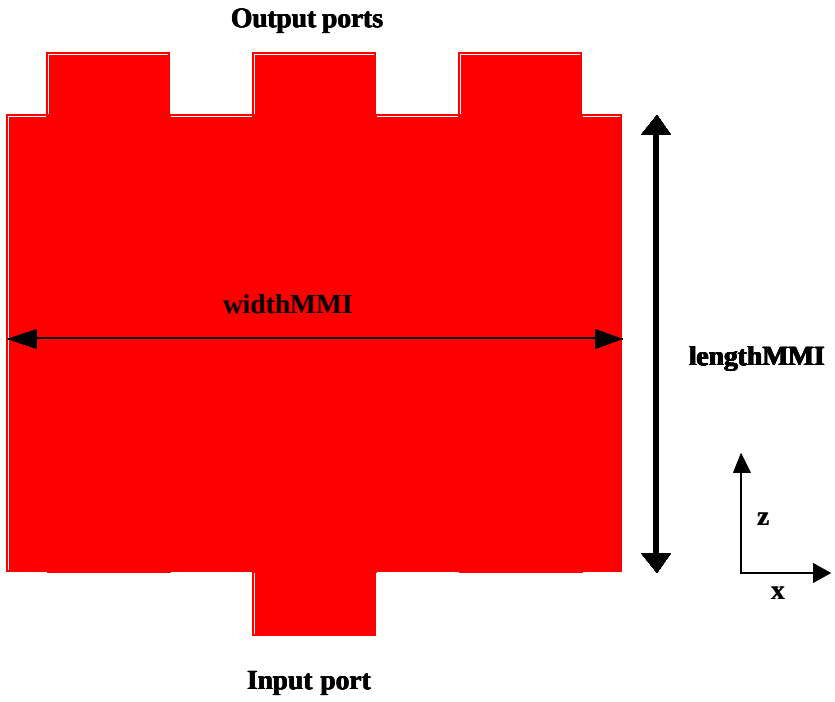

Figure 5.8: Geometrical layout of MMI coupler

5.3.1) Theoretical aspects

The following discussion is taken from [4]. For a one-dimensional description of the component, the effective index method may be used. The input field $F(x,0)$ is written as a sum of the slab modes $f(x)$, as in equation 5.8:

$$\Phi(x,0) \approx \sum_{m=0}^{M-1} C_m f_m(x) \tag{5.8}$$

with C_m representing the amplitude of the mth waveguide mode, defined in terms of the overlap integral as

$$C_m = \frac{\int \Phi(x) f_m(x) dx}{\sqrt{\int f_m(x)^2 dx}}. \tag{5.9}$$

The $f_m(x)$'s denote the eigenmodes of the slab waveguide. For accurate reproduction of the input field, a large number of modes is desired. The field that propagates along the z direction is then described as:

$$\Phi(x,z) = \sum_{m=0}^{M-1} C_m f_m(x) e^{-jb_m z} \tag{5.10}$$

with the b_m's representing the propagation constants of the M modes.

For strongly guided waveguides $k_{xm} = (m+1)p/W_e$ (where k_{xm} is the transverse wave vector defined in chapter 2), with m the mode number and W_e the effective width. For high contrast waveguides, $W_e \gg W$. The longitudinal propagation constant is $b_m^2 = n_s^2 k_0^2 - k_{xm}^2$, where n_s is the refractive index of the slab region. The paraxial approximation yields:

$$b_m \approx n_s k_0 - \frac{(m+1)^2 lp}{4W_e^2 n_s} \tag{5.11}$$

Note that b_0-b_1=$3\,lp/4W_e^2 n_s$. The beat length between the fundamental mode and first order modes is given by:

$$L_c \equiv \frac{p}{b_0 - b_1} \cong \frac{4n_s W_e^2}{3l} \tag{5.12}$$

Now the propagation constants are written as follows:

$$b_0 \approx n_s k_0 - \frac{p}{3L_c} \tag{5.13}$$

$$b_m \approx b_0 - \frac{m(m+2)p}{3L_c} \tag{5.14}$$

At a distance of $3L_c$, the modes have a relative phase that differs by an odd or even multiple of p depending on whether m is odd or even.

Due to the structural symmetry about x=0 (in the middle of the structure), the odd and even eigenmodes satisfy the following symmetry conditions:

$$f_m(x) = f_m(-x) \quad for\ even\ m$$
$$f_m(x) = -f_m(-x) \quad for\ odd\ m \tag{5.15}$$

Consequently, an output that is the mirror image of the input at $x=0$ occurs at a distance $z = 3L_c$. By assuming a large index contrast and slab modes with even and odd symmetry, a simple device model can be formulated, as in equation 5.15:

$$f_m(x) \approx \left\{ \begin{array}{l} \sin\left(\frac{px(m+1)}{W}\right) for\ odd\ m \\ \cos\left(\frac{px(m+1)}{W}\right) for\ even\ m \end{array} \right\} \tag{5.16}$$

Multiple images of the input are formed at intermediate lengths. At a distance of $3L_c/N$ from $z = 0$, there are N self-images with the qth image located at x_q, with phase f_q given as follows[2]:

$$x_q = (2q - N)\frac{W_e}{N} \tag{5.17}$$

$$f_q = q(N - q)\frac{p}{N} \tag{5.18}$$

for $0 \le q \le N - 1$. The total field at $z = 3L_c/N$ is given by

$$\Phi(x, \frac{3L_c}{N}) = \frac{e^{-jx}}{\sqrt{N}} \sum_{q=0}^{N-1} \Phi(x - x_q) e^{j f_q} \tag{5.19}$$

where $x = b_0 \frac{3L_c}{N} + p\left(\frac{1}{N} + \frac{N-1}{4}\right)$.

When an MMI is used as a splitter or a combiner in an interferometer, the phase relationships between the output ports are needed. These relationships are given in terms of the input waveguide [2]:

$$f_{ij} = -x + \frac{p}{4N}(j + i - 1)(2N - j - i + 1) \quad \text{for odd i + j} \tag{5.20}$$

$$f_{ij} = -x + \frac{p}{4N}(2N - j + i)(j - i) + p \quad \text{for even i + j.} \tag{5.21}$$

5.3.2) MMI design

The waveguide structure as defined in chapter 2 can be used for the manufacture of MMI couplers. The simulations yielded excellent results, underlining the fact that high index contrast waveguides are ideal for MMI couplers. In figure 5.8 the BPM simulation for the MMI coupler is shown. The light-blue and green coloured sections clearly indicate the position of the image points. A 1×2 structure was defined as a possible building block for a tuneable coupler utilising a Mach-Zehnder architecture as discussed in section 6.6, where an additional 2×2 MMI coupler is introduced.

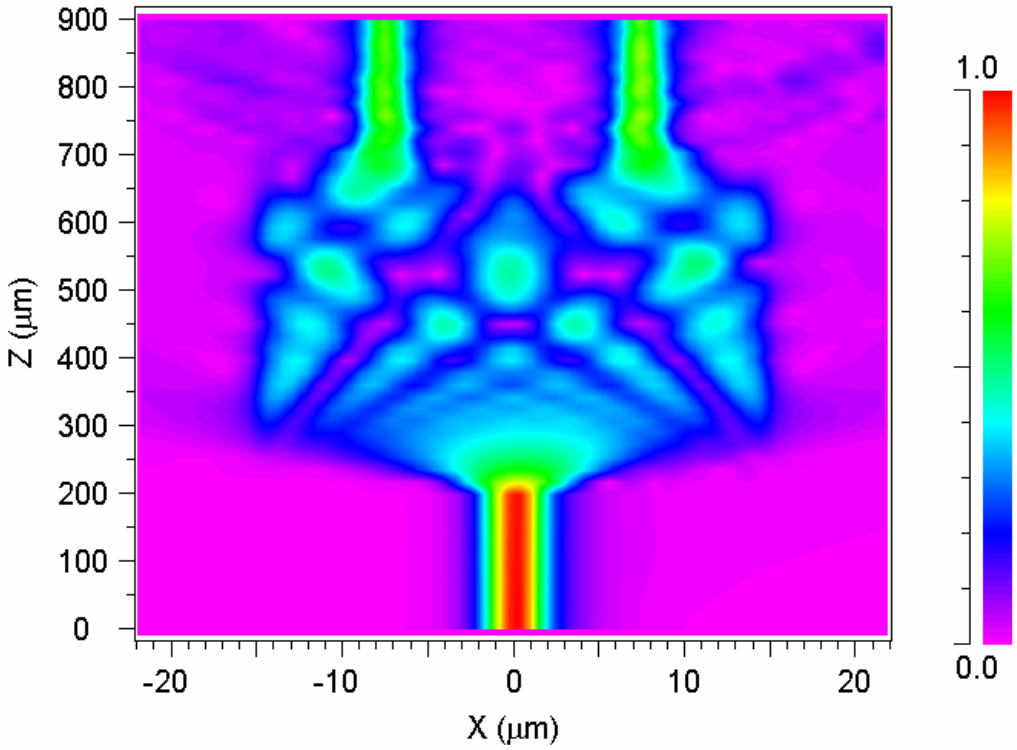

Figure 5.9: BPM simulation graphically depicting the MMI imaging process

In order to optimise the design, two-dimensional simulations were conducted first, as they have less computational time. The design parameters and results obtained for the designed two-dimensional MMI coupler are presented in Table 5.1. These parameters were optimised by running a series of simulations varying one parameter at a time.

The BPM simulation result is presented in figure 5.9. The values for the excess loss and output uniformity are very good in terms of MMIs. Lower losses can be achieved by introducing a taper to the MMI section, as presented in [9].

Input taper	4.5μm
Output taper	4.5μm
Input length	200μm
Output length	400μm
MMI length	479.2μm
MMI width	30μm
Excess loss	0.194dB
Maximum output non-uniformity	0.12dB

Table 5.1: Design parameters and results for two dimensional MMI coupler design

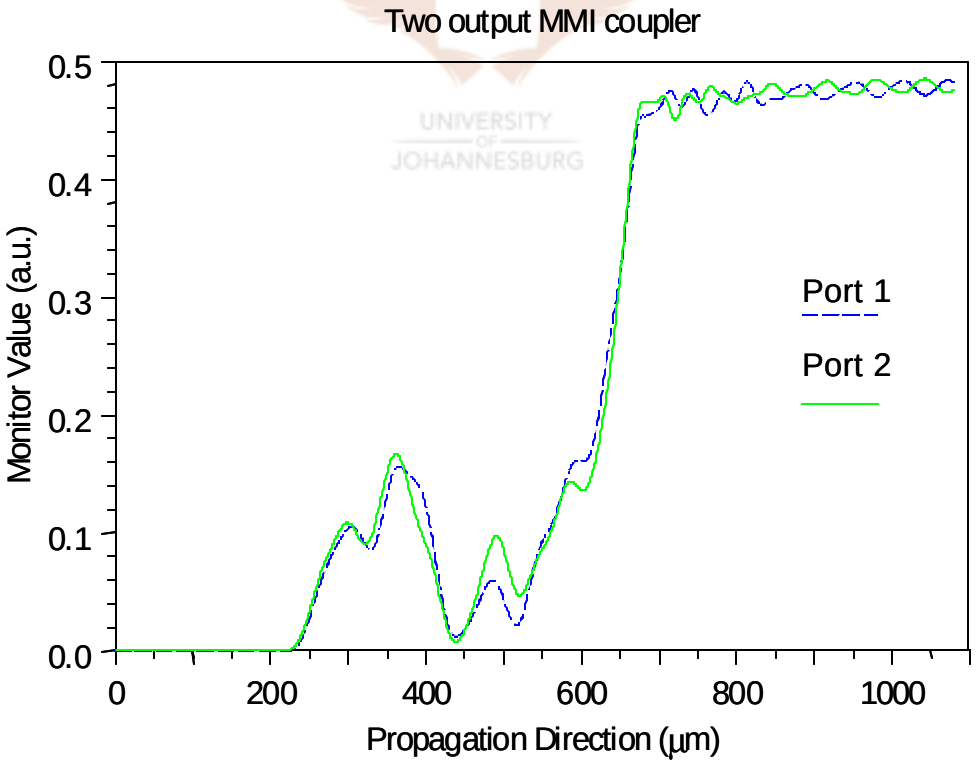

Figure 5.10: Simulation of the MMI coupler

The ripple observed in figure 5.9 at the output stage is due to mutual coupling between the two output waveguides. By using s-bends at the output, this effect can be minimised.

For the three-dimensional simulation, all of the above geometrical values were kept constant. The results obtained for excess loss was 0.55dB, whereas the maximum non-uniformity was 0.4dB. It is clear that the two-dimensional design yields results that are in the same order as the three-dimensional case. When it is considered that the two-dimensional simulation is markedly faster, it can be concluded that 2-D simulations can be used confidently when more integrated systems are investigated.

5.4) Star couplers

Star couplers are used as basic cross-connects in passive optical networks [5]. They consist of input and output arrays of waveguides separated by a slab diffraction region as shown in figure 5.11. Star couplers ideally couple the lightwaves from any input to all the outputs evenly and without wavelength selectivity.

Through the conservation of power, the minimum loss per port is 10log(N), where N is the number of output channels. This minimum loss is also known as the splitting loss [4]. The field distribution at the output array is the Fourier transform of the field at the input array [10]. A MATLAB program (and results obtained with it) that simulates the coupler by means of Fourier optics can be found in the appendix. In most cases, the number of output waveguides will exceed the number of inputs so as to ensure that the so-called Brillouin region is covered [5]. Furthermore, to make the outputs more uniform, the input waveguides are up-tapered near the slab region.

The layout used in figure 5.11 is the Rowland-circle geometry. It is a concave geometry with the advantage of allowing for coupling with linear fibre and detector arrays. A detailed description of the Rowland-circle is given in section 7.2 with specific reference to its use in arrayed waveguide grating (AWG) configurations. The chirping of these star couplers is also discussed in section 7.7.1.

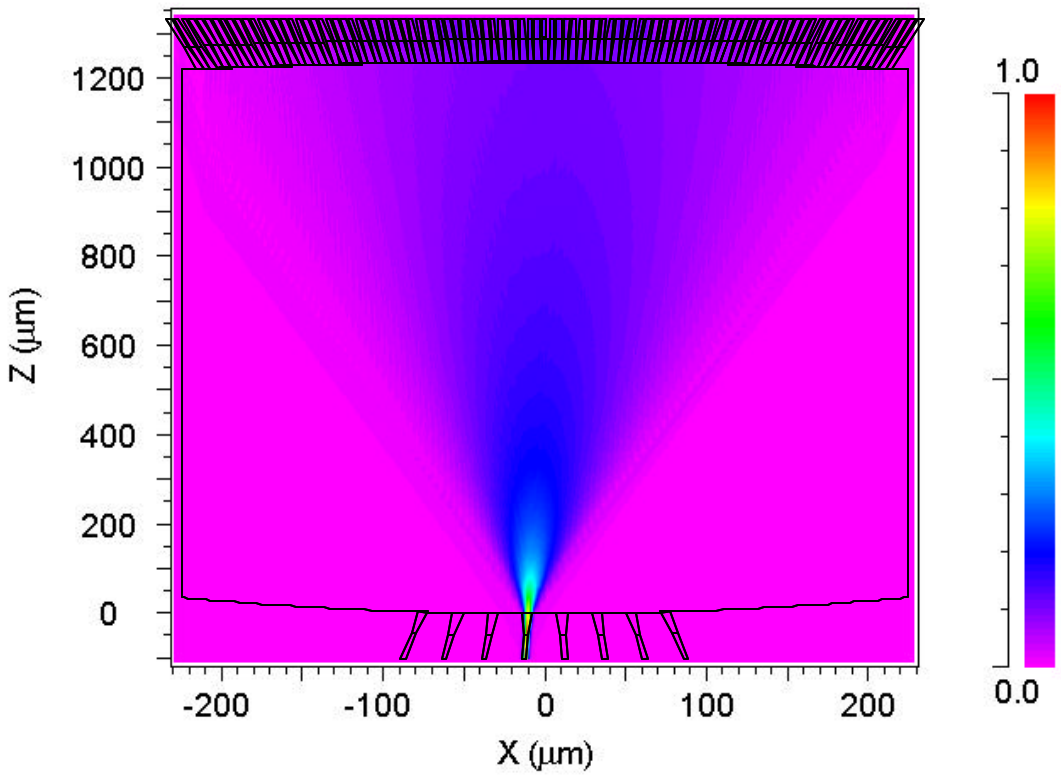

Figure 5.11: Geometrical layout of waveguide star coupler. The colour bar indicates the normalised light intensity

5.5) *Conclusions*

Couplers play a vital role in planar lightwave circuits. The selection of coupler types is based on the filter configuration to be used.

So for example, bi-directional couplers and MMI couplers can be used in tuneable coupler configurations. In general, the MMI couplers are more robust from a fabrication viewpoint, but exhibit higher excess losses. Extremely short MMI couplers (20µm – 30µm in length) have been demonstrated [4], which are advantageous when very short circuits are required.

Lattice MZI filters are built by using bi-directional couplers. The couplers designed for this purpose are as small as possible for direct simulation, but where smaller sizes are required, a method of prediction was presented in section 5.2.3. Because waveguide spacing plays the most significant role in directional couplers, the downscaling operation defined in section 5.2.3 is only valid if the spacing of the second segment of the s-bend is equal to the spacing of the coupler as simulated directly.

Star couplers are capable of splitting light in multiple waveguides without wavelength dependence. They allow for very high levels of integration as displayed in AWGs, and are sufficiently robust from a manufacturing viewpoint [10].

5.6) References

1) E.A.J. Marcatili, "Bends in optical dielectric guides", Bell Systems Technology Journal, vol. 48, pp. 2071 – 2102, 1969.
2) E.A.J. Marcatili, "Dielectric rectangular waveguide and directional couplers for integrated optics", Bell Systems Technology Journal, vol. 48, pp. 2071 – 2102, 1969.
3) N. Takato, K. Jinguji, M. Yasu, H. Toba, M. Kawachi, "Silica-based single-mode waveguides on silicon and their application to guided-wave optical interferometers", Journal of Lightwave Technology, vol. 6, pp. 1003 – 1010, 1988.
4) C.K. Madsen, J.H. Zhoa, "Optical filter design and analysis: A signal processing approach", Wiley interscience, 2000.
5) Y.P. Li, C.H. Henry, "Silica based optical integrated circuits", IEE Proceedings in Optoelectronics, vol. 143, pp. 263 – 280, 1996.
6) M. Smit, C. van Dam, "PHASAR-based WDM-devices: principles, design and applications", IEEE Journal of Selected Topics in Quantum Electronics, vol.2, pp. 236 – 250, 1996.
7) M.R. Amersfoort, "Phased-array wavelength demultiplexers and their integration with photodetectors", Delft university press, 1994.

8) L.B. Soldano, E. C. M. Pennings, "Optical multi-mode interference devices based on self-imaging: Principles and applications," Journal of Lightwave Technology, vol. 13, pp. 615 – 627, 1995.
9) T. Augustsson, “Bragg grating-assisted MMI-coupler for add-drop multiplexing”, Journal of Lightwave Technology, vol. 16, pp. 1517 – 1522, 1998.
10) K. Okamoto, “Recent progress of integrated optics planar lightwave circuits”, Optical and Quantum Electronics, vol. 31, pp. 107 – 129, 1999.